Biochimica et Biophysica Acta 1840 (2014) 2128–2138

Contents lists available at ScienceDirect

Biochimica et Biophysica Acta

journal homepage: www.elsevier.com/locate/bbagen

Molecular modeling study on the dynamical structural features of human smoothened receptor and binding mechanism of antagonist LY2940680 by metadynamics simulation and free energy calculation

Qifeng Bai [a], Yulin Shen [b], Nengzhi Jin [b], Huanxiang Liu [c], Xiaojun Yao [a,d,*]

[a] College of Chemistry and Chemical Engineering, Lanzhou University, Lanzhou, Gansu 730000, PR China
[b] Gansu Computing Center, Lanzhou, Gansu 730000, PR China
[c] School of Pharmacy, Lanzhou University, Lanzhou, Gansu 730000, PR China
[d] State Key Laboratory of Quality Research in Chinese Medicine, Macau Institute for Applied Research in Medicine and Health, Macau University of Science and Technology, Taipa, Macau, PR China

ARTICLE INFO

Article history:
Received 2 January 2014
Received in revised form 26 February 2014
Accepted 10 March 2014
Available online 15 March 2014

Keywords:
Smoothened receptor
Molecular dynamics simulation
Metadynamics
Free energy calculation
GPCR

ABSTRACT

Background: The smoothened (SMO) receptor, one of the Class F G protein coupled receptors (GPCRs), is an essential component of the canonical hedgehog signaling pathway which plays a key role in the regulation of embryonic development in animals. The function of the SMO receptor can be modulated by small-molecule agonists and antagonists, some of which are potential antitumour agents. Understanding the binding mode of an antagonist in the SMO receptor is crucial for the rational design of new antitumour agents.
Methods: Molecular dynamics (MD) simulation and dynamical network analysis are used to study the dynamical structural features of SMO receptor. Metadynamics simulation and free energy calculation are employed to explore the binding mechanism between the antagonist and SMO receptor.
Results: The MD simulation results and dynamical network analysis show that the conserved KTXXXW motif in helix VIII has strong interaction with helix I. The α-helical extension of transmembrane 6 (TM6) is detected as part of the ligand-binding pocket and dissociation pathway of the antagonist. The metadynamics simulation results illustrate the binding mechanism of the antagonist in the pocket of SMO receptor, and free energy calculation shows the antagonist needs to overcome about 38 kcal/mol of energy barrier to leave the binding pocket of SMO receptor.
Conclusions: The unusually long TM6 plays an important role on the binding behavior of the antagonist in the pocket of SMO receptor.
General significance: The results can not only profile the binding mechanism between the antagonist and Class F GPCRs, but also supply the useful information for the rational design of a more potential small molecule antagonist bound to SMO receptor.

1. Introduction

G protein coupled receptors (GPCRs), a large family of seven transmembrane domain receptors, were the targets of approximately 40% of modern drugs [1]. The GPCRs were generally classified into six main families on the basis of sequence and structure similarity: class A (rhodopsin-like), class B (secretin receptor family), class C (metabotropic glutamate/pheromone), class D (fungal mating pheromone receptors), class E (cyclic AMP receptors) and class F (frizzled/smoothened) [2–8]. More than 18 structures of class A receptors of GPCRs have been determined to understand the structure and function of GPCRs [9]. Two class B GPCRs have been solved: the corticotropin-releasing factor receptor 1 (CRF_1R) [2] and glucagon receptor (GCGR) [10]. Among different GPCRs, the smoothened (SMO) receptor, an important member of class F GPCRs in the hedgehog signaling pathway, played an important role in the maintenance of embryonic development in animals [11,12]. The SMO receptor was reported to couple with G protein and its function could be modulated by the natural or synthetic antagonists and agonists [13]. SMO receptor shared less than 10% sequence identity with class A GPCRs and had most features of the class frizzled GPCRs [8,14]. However, the crystal structure of SMO receptor, which was solved recently to study the binding mode of a potential antitumour agent to SMO receptor, showed a highly similar spatial conformation with the Class A GPCRs [15]. The crystal structure of SMO receptor in complex with LY2940680 illustrated that the ECL structure, ECD linker domain and α-helix structure formed the antagonist-binding domain [15]. The antagonist LY2940680 competed with binding of the inverse

* Corresponding author at: College of Chemistry and Chemical Engineering, Lanzhou University, Lanzhou, Gansu 730000, PR China. Tel.: +86 931 891 2578; fax: +86 931 891 2582.
E-mail address: xjyao@lzu.edu.cn (X. Yao).

http://dx.doi.org/10.1016/j.bbagen.2014.03.010
0304-4165/

agonist Cyclopamine [16] and agonist of SAG [15] in the long and narrow pocket of SMO receptor.

The recently reported crystal structure of SMO receptor provided some static information about the interaction between SMO receptor and antagonist LY2940680. But more details about the dynamical interaction and its modulation mechanism such as free energy, the dissociation pathway of the antagonist were still elusive. Molecular modeling methods such as molecular dynamics (MD) simulations combined with principal component analysis, clustering analysis, cross-correlation analysis and dynamical network analysis could help us to understand the binding and modulation mechanism of the antagonist on SMO receptor at the atomic level. In addition, on the basis of molecular dynamics simulation, free energy calculation, potential mean force and dynamical network analysis could also be used to predict the binding affinity of the antagonist upon SMO receptor and to identify the key residues of protein, which were useful for the structure based drug design of new potent modulators [17,18].

During the past years, many molecular modeling studies about the class A GPCRs had been reported using the MD simulations on the basis of the crystal structures. For instance, the β_2 adrenergic receptor (β_2AR) in complex with the agonist, antagonist and inverse agonist had been studied using MD simulations and molecular docking. The results of MD simulations proved that there were different interaction modes between β_2AR and different kinds of ligands [19–21]. The dissociation pathway of ligands in the pocket of β_2AR was also identified using MD simulations [22,23]. Free energy calculations were also used to profile different landscapes of ligands bound to the β_2AR by adaptive biasing techniques [24] and metadynamics simulations [25–29]. Besides, the dynamical transform between the active and inactive states of β_2AR was reported by long molecular dynamics simulations [30,31]. In addition, the interaction between β_2AR and Gs protein was studied for the activation mechanism of β_2AR and other GPCRs using MD simulations [32]. The results of molecular docking and MD simulations illustrated that only the inverse agonist could induce the separation of Gαs and Gβγ indirectly though changing the conformation of β_2AR [20]. Furthermore, the molecular modeling methods combined with the biological experiments, were successfully used to discover the active compound of β_2AR [33]. Until now, there was no report about the analysis of antagonist-bound SMO receptor using MD simulations and free energy calculations.

In the present study, we utilized a combination of computational techniques including molecular dynamics simulations, free energy calculations, and metadynamics simulations to generate an ensemble view of the dynamic properties of the binding mechanism of SMO receptor with its antagonist LY2940680. MD simulations were carried out to study the dynamical structural features of SMO receptor and the interaction between the antagonist and the SMO receptor. The dynamical network analysis was also used to explore the interaction mode between the antagonist and SMO receptor. The metadynamics simulations were used to calculate the energy surface with respect to the reaction coordinate of a dihedral angle in LY2940680. The free energy calculation from adaptive biasing force (ABF) simulations was used to depict the energy barrier and energy deep well along the reaction coordinate. The simulation results could provide some information about the function of important domain and key residues of SMO receptor as well as the behavior of antagonist LY2940680 in the protein pocket. Our study could give valuable insights into the binding and modulation mechanism of SMO receptor and provide some useful clues for the design of small molecules by targeting the SMO receptor.

2. Materials and methods

2.1. Protein preparation

The crystal structure of SMO receptor in complex with antagonist LY2940680 was obtained from the PDB database (PDB code: 4JKV [15]). The subunit A of the crystal model of SMO receptor was saved to build a receptor model. Besides, the antagonist LY2940680 and crystal water were stored to construct the complex and to study the interaction mode. The thermostabilized apocytochrome b_{562}RIL (BRIL) was saved to replace the extracellular cysteine-rich domain (CRD) (see Fig. 1A) [15]. The explicit membrane around the hydrophobic part of SMO receptor was built by 1-palmitoyl-2-oleoyl-sn-glycero-3-phosphocholine (POPC) lipids using VMD [34] soft package. The final size of the membrane was about 75 Å × 75 Å. The TIP3P water [35] was used to fill in the periodic boundary box with a size of 75 Å × 75 Å × 100 Å. To get the neutral environment of the entire system, two sodium ions were immersed into the water. The whole system, which included the SMO receptor, antagonist, water, lipids and ions, had a total of ~40,000 atoms per periodic cell. The web server SwissParam [36] was used to construct the CHARMM force field parameters of antagonist LY2940680.

2.2. Molecular dynamics simulations

The above built complex was used to perform molecular dynamics (MD) simulations. First of all, only the lipid tail was relaxed freely in 100 ps minimization and was equilibrated with 500 ps at constant temperature (310 K) and constant pressure (1 bar). Then, all atoms except SMO receptor and the antagonist were relaxed for a minimization of 100 ps and equilibration of 500 ps. Subsequently, a 10 ns MD simulation was run on the whole system without any constrain to get the equilibrated phase. At last, 50 ns product MD simulations were performed on the SMO receptor and antagonist in explicit lipids and water.

All the simulations were carried out under a constant pressure of 1 bar and a constant temperature of 310 K. The minimization was based on the conjugate gradient method. The electrostatics potential was calculated with a nonbonded cutoff of 12 Å based on the particle-mesh Ewald (PME) [37] method. The constant temperature and pressure were calculated by the langevin thermostat [38,39] and langevin barostat [40] method, respectively. All the MD simulations were performed with a time step of 2 fs. The trajectories of MD simulations were stored every 5 ps for the analysis of MD simulated data. All the MD simulations were carried out using NAMD [41] (version 2.9b3) on 12 cores of an array of two 2.66-GHz Intel Xeon 5650 processors and 4 pieces of NVDIA Tesla C 2050 graphics card.

2.3. Dynamical network analysis

The dynamical network analysis was used to build network model of the residues of SMO receptor and to find the potential strongest interaction residues in the receptor. The network model was built by the NetworkView plugin of VMD [34,42,43] and the program Carma [44]. In the network, the nodes could be considered as one single atom or coarse grained representation of a residue. Here, the position of each node was defined at the center of Cα atom of amino acid. One node in the network represented one residue of protein. The edge between two nodes was defined with the cutoff distance of 4.5 Å for at least 75% of MD simulated trajectory. The edge distance was defined as Eq. (1):

$$d_{ij} = -\log\left(\left|C_{ij}\right|\right) \tag{1}$$

where C_{ij} represented pairwise correlations which were obtained by the calculation of the program Carma [44].

2.4. The potential of mean force (PMF)

To study the energetic change accompanied with the structural fluctuation of SMO receptor, the potential of mean force (PMF) was considered as a useful method for the generation of energy landscape. The PMF

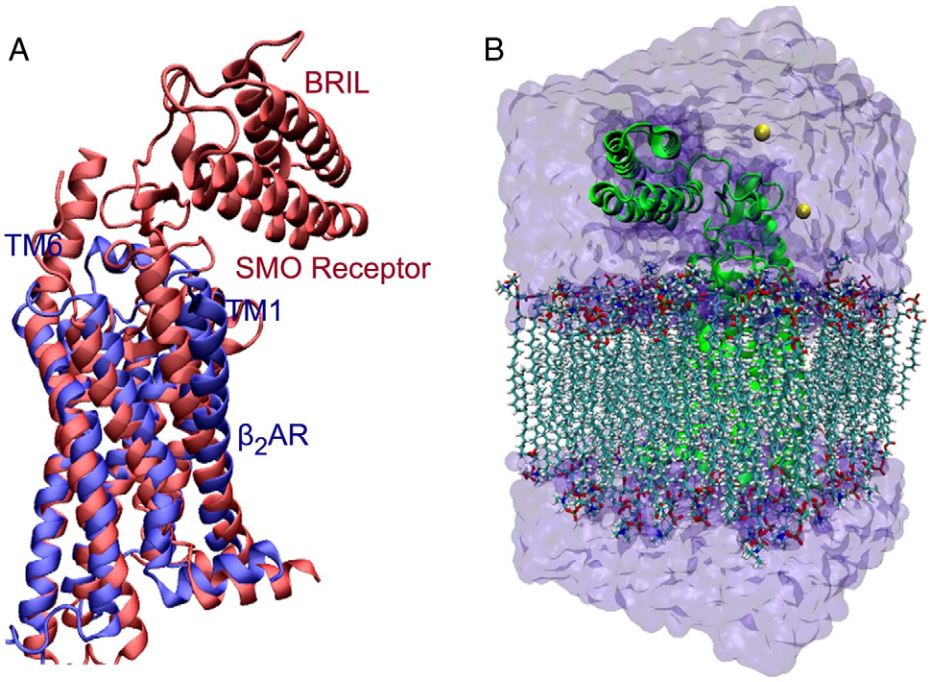

Fig. 1. The model of SMO receptor. (A) Conformational alignment between SMO receptor (PDB ID: 4JKV [15]) and β_2AR (PDB ID: 3NYA [58]). (B) The MD simulated model of SMO receptor in complex with the antagonist LY2940680 in explicit lipids, water and ions.

which was used to describe an average over all the conformation of protein indicated the preferential conformation of protein during MD simulations. The PMF was calculated by the Eq. (2) [45–47]:

$$\Delta G(x,y) = -k_B T \ln g(x,y) \tag{2}$$

where k_B and T represented the Boltzmann constant and MD simulated temperature respectively. The $g(x,y)$ was the normalized joint probability distribution. The x and y represented the principal component 1 (PC1) and principal component 2 (PC2) obtained from the Cartesian principal component analysis (PCA) on basis of covariance matrix using the program Carma [44].

To calculate the hydrogen bond occupancy, the distance and the angle between the donor and acceptor were set to 3.7 Å and 35° respectively [48,49]. The radial distribution function (RDF) $g(r)$ could compute the probability between two particles along the reaction coordinate. The $g(r)$ could be calculated as Eq. (3) [50]:

$$g(r) = 4\pi r^2 dr \tag{3}$$

where r represented the distance between waters and the pointed residues of SMO receptor.

2.5. Metadynamics simulations

Metadynamics [51] was used in MD simulations to improve the sampling space and to find the free energy surface. It was similar to other free energy calculation methods such as umbrella sampling [45,52] and adaptive biasing force (ABF) [53–55] method. Gaussian potential was used in metadynamics to fill the free energy wells. If the energy landscape of a system was not explored fully, the component of forces would let the discouraged system come back to the previous spot. The full energy landscape could be obtained by the opposite sum of the Gaussians in the reaction coordinate. Because the width and height of the Gaussian potential could be adjusted according to the real situation, metadynamics simulation was convenient to optimize the ratio of computational cost and accuracy. In addition, metadynamics simulations could calculate the free energy at the classical and quantum level, and it has been successfully applied to study the conformational change mechanism of chemical molecules and biologic macromolecules [56]. The free energy $V(s)$ of metadynamics could be evaluated as Eq. (4):

$$-\sum_{t_1 \le t} We^{-\frac{|\sigma - \sigma t_1|^2}{2\delta\sigma^2}} \rightarrow V(s) \tag{4}$$

where the width and height of the Gaussian W and the $\delta\sigma$ represented the reasonable compromise of accuracy and efficiency in the free energy surface. Here, the dihedral angles of θ_1 and θ_2 of the antagonist LY2940680 were rotated from −180 to 180° to obtain the free energy surface of LY2940680 in SMO receptor with explicit lipids and water (see Fig. 7A). Besides, to study the free rotation of dihedral angles of the antagonist LY2940680 in the solvate environment, the water box, with a size of $21 \times 18 \times 27$ Å^3, was built with the TIP3P water model. The antagonist LY2940680 was immersed into this water box. The width and height of the Gaussian potential were both set to 1.25 and 0.1 kcal/mol, respectively. The PMF was saved every 1000 frames with 1.0 Å/bin periodically. And the new hill was added into the old dependent potential every 100 steps. Both of the systems performed 50 ns metadynamics simulations.

2.6. Free energy calculation by adaptive biasing force

Free energy calculation played an important role to study the dynamical interaction between the ligands and protein. The adaptive biasing force (ABF) [53–55] method was used in the present work to profile the free energy of the antagonist along the reaction coordinate. The ABF method could offset the local barriers to make all the reaction coordinate sampling with equal probability. Especially, ABF could improve the accuracy of free energy calculation through a reversible process along the pointed reaction coordinate. The free energy ΔG was defined from the state a to b as shown in Eq. (5):

$$\Delta G_{a\rightarrow b} = -\int_{\xi_a}^{\xi_b} F_\xi d\xi \tag{5}$$

where F_ξ was the biasing force. Our model was built along the Z axis. As shown in Fig. S2, the antagonist LY2940680 was located in the long and

narrow pocket. Because the pocket channel of SMO receptor was open along the positive Z axis, the free energy of LY2940680 along the positive Z axis was computed in our work. To stretch out of the antagonist in the pocket of SMO receptor, the reference point was chosen as the center of T241, V276, A327, F369, G409, I465 and M525. The span of the reaction coordinate of the ABF algorithm could be divided into equally different lengths. Each divided length of the reaction coordinate was considered as one window. More divided windows of the reaction coordinate could enhance the ABF simulations effectively [57]. The 5 Å/windows and 0.2 Å/bin were set for the five non-overlapping windows along the reaction coordinate. The 20 ns MD simulations were performed on each window. A total of 100 ns MD simulations were run on the five windows. The wall force constant of 10 kcal/mol/Å^2 was applied to the boundary potential. The number of samples in a bin prior to biasing was set to 500. The ABF simulations were implemented in NAMD (version 2.9b3) [41] software package.

3. Results and discussion

3.1. Structural features of SMO receptor

The SMO receptor was the first class F GPCR with its crystal structure available. It was significant to understand its structural features by comparing the structure of SMO receptor with class A GPCRs. The structural alignment between SMO receptor (PDB ID: 4JKV [15]) and class A GPCR (β_2AR) (PDB ID: 3NYA [58]) showed that most of the transmembrane (TM) segments of SMO receptor were superposed well with the crystal structure of β_2AR. Exceptionally, the SMO receptor showed different superposed conformations in the TM1 and TM6 with β_2AR (see Fig. 1A). β_2AR had slightly expanded TM1 relative to SMO receptor. The main reason was that TM1 of SMO receptor was connected to an extracellular domain (ECD) linker domain (see Figs. 1A and 2A) compared with β_2AR. Another obvious difference was that the TM6 of SMO receptor had an extra α-helical extension. In the crystal structure of SMO receptor, it had seven transmembrane segments from the α-helix structure. Seven TMs (TM1–7) corresponded to the conformation of seven helixes (I–VII) (see Fig. 2A and D). The helix VIII was in the intracellular part of SMO receptor (see Fig. 2B). The ECD linker domain, which had a disulfide bond between C193 and C213, formed the kink structure in favor of the stability of structure. The extracellular loop (ECL) 1 between TM2 and TM3, which formed a disulfide bond between C295 and C217 of ECD linker domain, had a short α-helix before C295. The ECL2 between TM4 and TM5, which had a disulfide bond between C314$^{3.25}$ and C390, contained a β-hairpin for the pocket formation of SMO receptor. The fourth disulfide bond was formed by C490 and C507 of ECL3. The ECL3 between TM6 and TM7 was mostly disordered (see Fig. 2A). The integrity of the ECL conformation, which was connected by disulfide bonds to each other, was necessary to keep the SMO receptor in a stable state [15,59].

To further study the binding mode of the antagonist to SMO receptor, the SMO receptor in complex with antagonist LY2940680 was immersed into the lipids and water box and neutralized by two sodium ions (see Fig. 1B). 50 ns MD simulations were performed to study the binding mode of the antagonist LY2940680 in the pocket of SMO receptor. After 50 ns MD simulations, the simulated structure superposed with the crystal structure well (see Fig. 2B). The root mean square deviation (RMSD) showed that the TM1–7 of SMO receptor got into the equilibrium phase in 50 ns MD simulations. Although the ECD linker

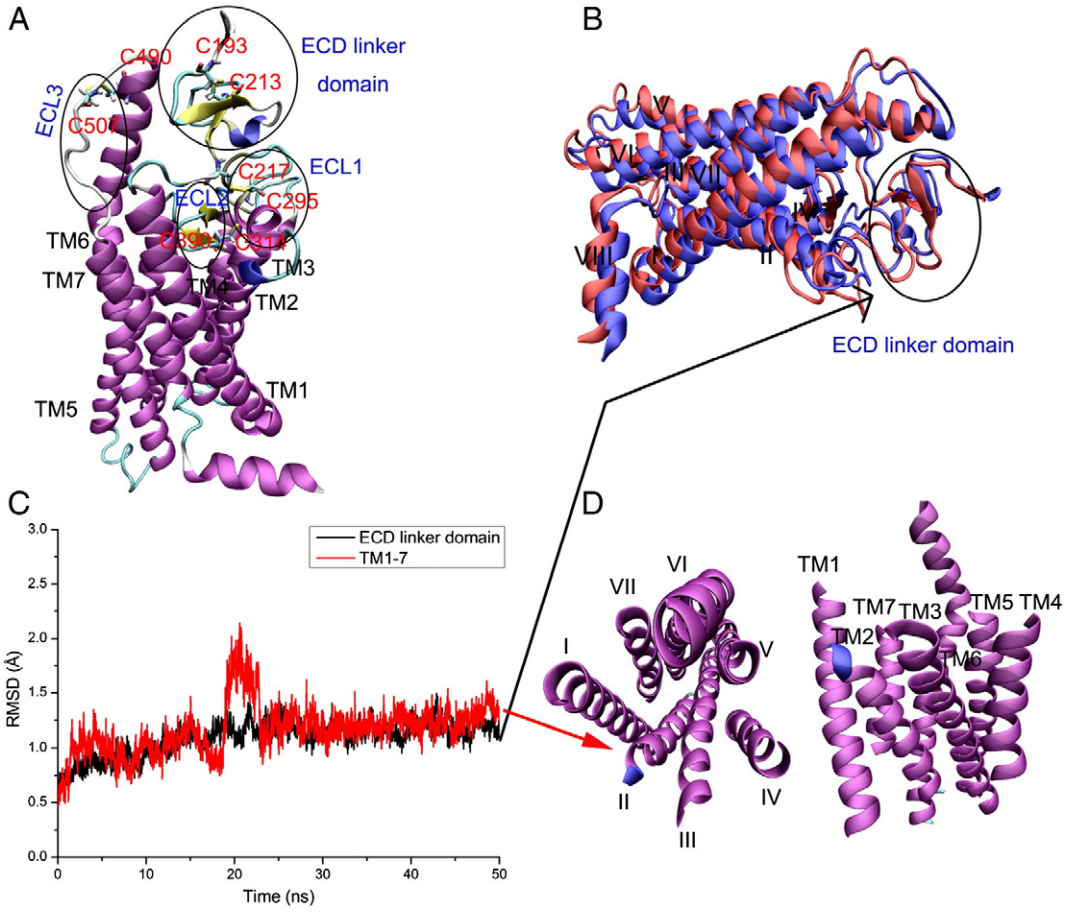

Fig. 2. Structural features of SMO receptor. (A) The domains of SMO receptor. (B) Conformational superposition between the simulated equilibrium structure and crystal structure of SMO receptor. (C) The RMSD of backbone atoms of ECD linker domain and TM1–7. (D) The representation of transmembrane segments (TM1–7) corresponding to helixes I to VII.

domain was considered as the disordered structure, the RMSD of backbone atoms of the ECD linker domain kept about 1.1 Å stably in 50 ns simulated time (see Fig. 2C). It indicated that the ECD linker domain packaged as a tight whole system during the MD simulations.

3.2. The analysis of key residues of SMO receptor

As shown in Fig. 3A, the RMSD of backbone atoms of SMO receptor proved that the conformation of SMO receptor was in a stable dynamical state. There was no NPXXY motif in SMO receptor which existed in helix VII of class A GPCRs. However, the KTXXXW motif in helix VIII of SMO receptor was instead of the NPXXY motif for the critical activation of signaling pathway. The conserved KTXXXW motif, which had a stable RMSD, suggested that the SMO receptor was still in the inactive state [15]. The residues T541, I544 and W545 in helix VIII of SMO receptor interfaced with the residue T251$^{1.56}$ and A254 in helix I. Especially, the hydrogen moiety of T541 of KTXXXW motif formed a hydrogen bond with the oxygen moiety of V536 in the intracellular end of helix VII, and the indole hydrogen of W545 had a hydrogen bond with the oxygen group of T251$^{1.56}$ in helix I. Besides, the residue T541 formed hydrogen bonds with the residues A540 and I544 (see Fig. 3B). The RMSD of the residues T251$^{1.56}$, A254, V536, K539, A540, T541, L542, L543, I544 and W545 calculated by vmdICE program [60], showed the conformational change of each residue during 50 ns MD simulations. The T251$^{1.56}$, A254 and V536 had a different conformational fluctuation with the conserved KTXXXW motif, and the residues of KTXXXW motif also had different RMSDs such as L542 and L543 because the L542 and L543 in the flank of helix VIII did not form hydrogen bonds with other transmembrane segments (see Fig. 3B and C).

To further study the interactions of the residues of SMO receptor, the dynamical network analysis was a useful method to explore potentially important interaction residues of SMO receptor. The dynamical network dealt with the nodes using a coarse grain model. Each node could represent a residue or an atom. According to the motion property of nodes, the dynamical network analysis could divide the network into different subnetworks which tuned into different colors. As shown in Fig. 4, the SMO receptor was built with different nodes and connected by different edges. The different color domains in SMO receptor represented different network communities. Interestingly, the strongest edges were distributed in helix VIII and helix I which formed the conserved structure in SMO receptor. In helix I, the strongest residues of A250$^{1.55}$, V253, T251$^{1.56}$, A254, F252 and D255 were connected to each other in turn. It did not form the complex connected network. In helix VIII, four residues of the conserved KTXXXW motif formed the strongest edges. The R546 formed the strongest edges with L542, L543 and I544 which corresponded to the "XXX" part of the KTXXXW motif. Another R547 only formed the strongest edges with I544. The main kink residue was the I544 of KTXXXW motif which had the strongest edges with L542, R546 and R547. The W545 had a strong edge with L542 as well as a hydrogen bond with T251$^{1.56}$ in helix I (see Figs. 3B and 4). The results of dynamical network analysis indicated that helixes I and VIII contained the conserved domain and supplied the interaction network of conserved residues of helixes I and VIII.

Since the conformational fluctuation was studied, the free energy of conformation of SMO receptor was necessary to be explored during the MD simulations. The potential of mean force (PMF) could be used to identify the conformational change of protein with the MD simulations. To decrease the dimensions of MD simulated results for PMF analysis, principal component analysis (PCA) on the basis of covariance matrix was employed to extract the major fluctuation property from the MD simulation trajectory of SMO receptor. The principal component 1 (PC1) and principal component 2 (PC2), which were measured by

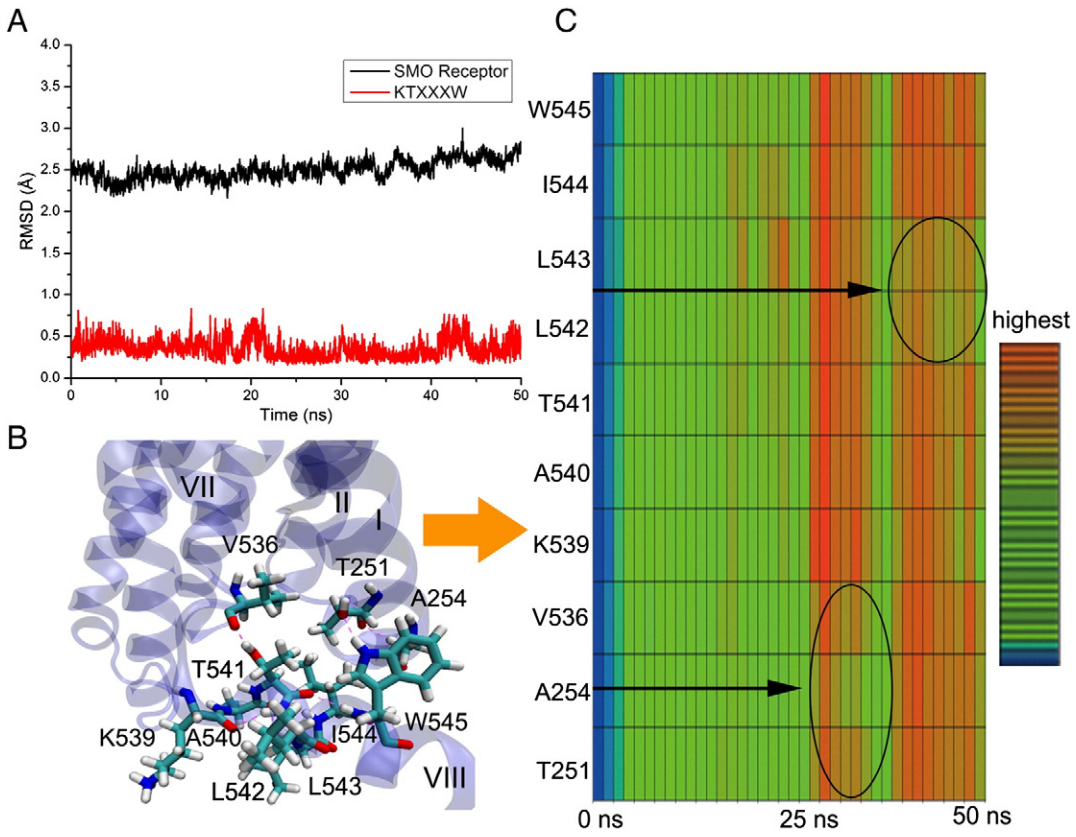

Fig. 3. Key residues of SMO receptor. (A) The RMSD of backbone atoms of SMO receptor and the conserved motif KTXXXW. (B) The representation of the motif KTXXXW and T251$^{1.56}$, A254 and V536. The SMO receptor had an extra A540 between the K539 and T541, the rest of motif of KTXXXW was conserved. (C) The RMSD of backbone atoms of the KTXXXW motif and T251$^{1.56}$, A254 and V536.

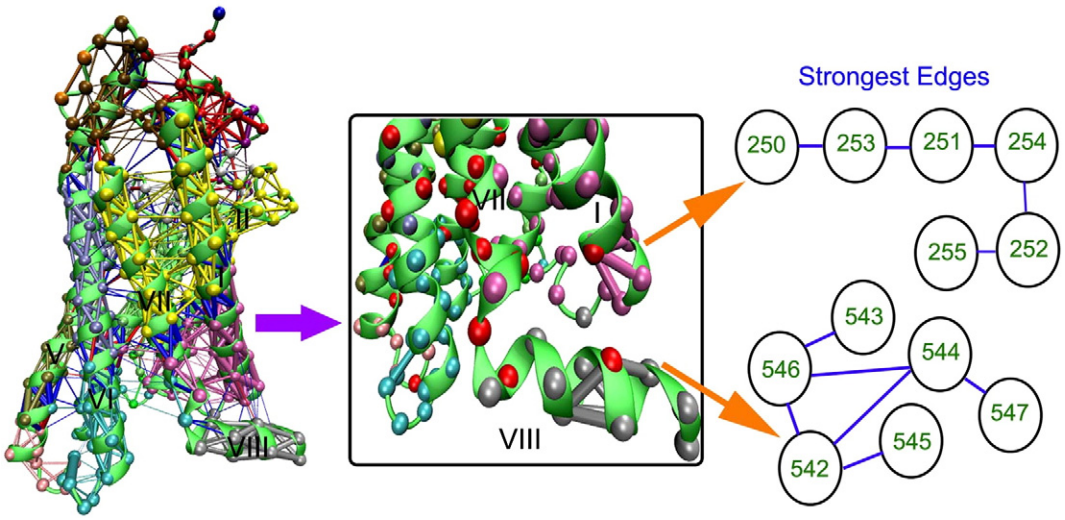

Fig. 4. Dynamical network analysis. The different color domains of SMO receptor represented different network communities. The points in the SMO receptor were the nodes, and the line between the nodes represented the edges. The thick lines showed the strong edges. The strongest edges were in the intracellular part of helixes I and VIII.

program Carma, could represent the most fluctuation of protein [61]. As shown in Fig. 5A, the PMF was calculated with respect to PC1 and PC2. There was only one energy deep well in the energy landscape along the two dimensional reaction coordinates. It indicated that the SMO receptor was in an inactive state stably during MD simulations. The RMSD and energy distribution of PMF corresponded to the conformational fluctuation of SMO receptor and was described in Figs. 3A and 5A.

The energy landscape indicated that SMO receptor kept a stable conformation. However, in the crystal structure of SMO receptor, TM6 had an unusually long α-helical extension part in the ECL3. To study

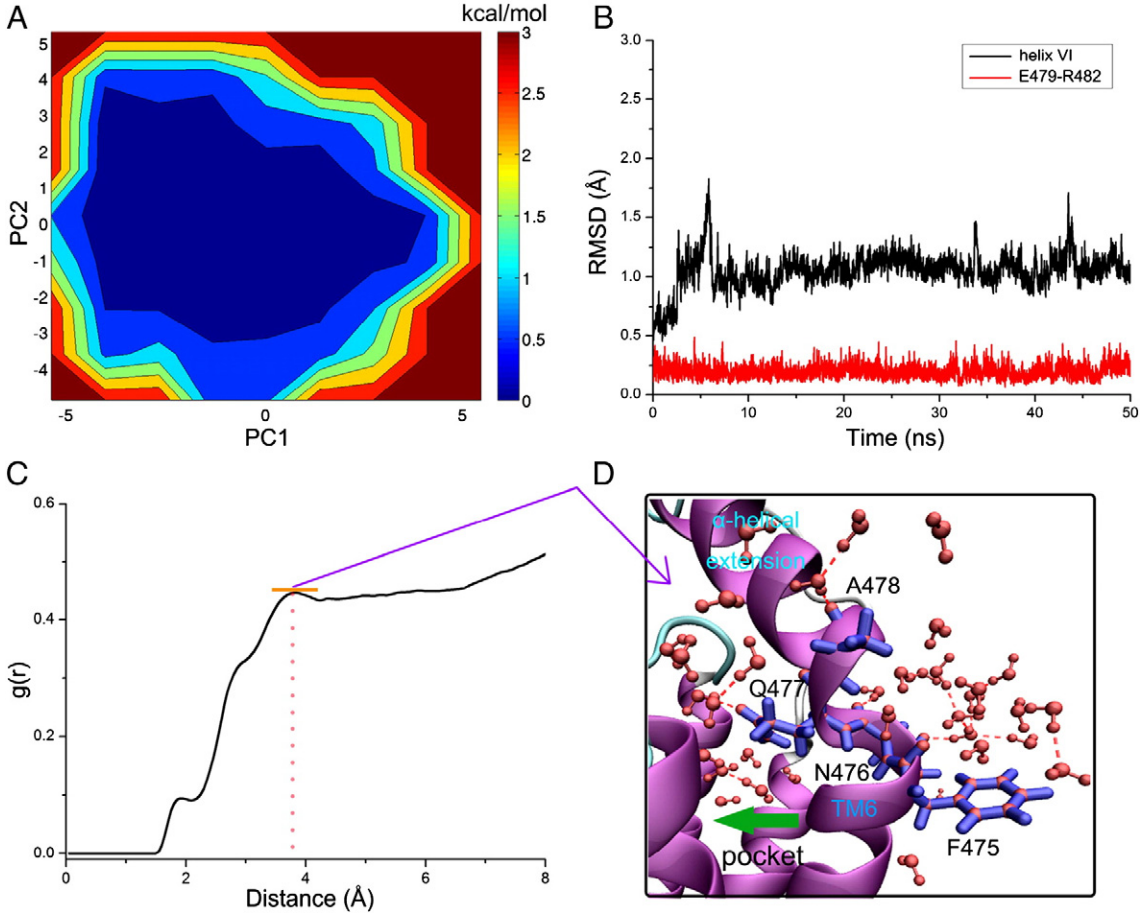

Fig. 5. PMF and the structure features of TM6. (A) The potential of the mean force of the conformation of SMO receptor with respect to PC1 and PC2. (B) The RMSD of backbone atoms of helix VI and E479–R482. (C) The radial distribution function $g(r)$ between the waters and F475, N476, Q477, A478. (D) The hydrogen-bonding network stabilized the non-proline kink at the connection of α-helical extension of TM6.

the conformational stability of helix VI which included TM6 and the α-helical extension of TM6, the RMSD of backbone atoms of helix VI was measured over the simulation time (see Fig. 5B). The RMSD indicated that the conformation of helix VI kept stable during 50 ns MD simulations. It indicated that the α-helical extension of TM6 was not distorted during MD simulations. The first reason was that the long extension of TM6 was partially stabilized by the ionic interaction between E479 and R482 [15]. As shown in Fig. 5B, the RMSD of backbone atoms of E479 and R482 suggested that the ionic interaction of E479 and R482 kept stable during the MD simulations. The second reason was due to the hydrogen bond network between the water molecules and F475, N476, Q477, A478 which could stabilize the non-proline kink of the α-helical extension and TM6 (see Fig. 5D).

To explore the distribution of water molecules around residues F475, N476, Q477 and A478, radial distribution function (RDF) was used to calculate the possibility along the reaction distance between the water molecules and residues F475, N476, Q477, A478. As shown in Fig. 5C and D, water molecules were located in a pocket of SMO receptor and out of helix VI. When the reaction distance was ~3.7 Å, the $g(r)$ had a peak corresponding to the formation distance of hydrogen bonds. In this reaction distance, water molecules formed dynamical hydrogen bonds with residues F475, N476, Q477 and A478. After the reaction distance of ~3.7, the $g(r)$ slightly decreased because the number of water was limited in the pocket of SMO receptor and the water molecules were uniformly distributed in the solvate box. With the increase of reaction distance, more water molecules of the solvate box were counted and this led to the high value of the $g(r)$. The RDF results indicated that the hydrogen bond network was formed around the non-proline kink of the α-helical extension of TM6.

3.3. The interaction between antagonist LY2940680 and SMO receptor

The hydrogen bond occupancy analysis was performed to find important residues which had high frequency hydrogen bond interaction with the antagonist LY2940680 during the MD simulations. The residue N219, which anchored in the ECD linker domain, had high hydrogen bond occupancy. Besides, the residue L221 of the ECD linker domain also formed hydrogen bonds with the antagonist LY2940680 (see Figs. 6A, B and S1). It indicated that the ECD linker domain played an important role in the formation of a ligand-binding pocket. The residues K395, Y394, S387 and D384 of ECL2 formed hydrogen bonds with antagonist LY2940680. Remarkably, the D384 residue located in the β-hairpin of ECL2 was in a deep position of the extracellular part of SMO receptor. The residues of ECL1 did not form the hydrogen bonds with the antagonist LY2940680 because it was far away from the pocket of SMO receptor. There was one hydrogen bond between P513 of the disordered part of ECL3 and antagonist LY2940680. Especially, the residues Q477, W480, E481 and F484 in the α-helical extension of TM6 formed four hydrogen bonds with the antagonist LY2940680. In addition, the residues in the helixes of SMO receptor also formed hydrogen bonds with antagonist LY2940680. The W281$^{2.57}$ of helix II, R400$^{5.39}$ of helix V and E518$^{7.38}$ of helix VII could form the dynamical hydrogen

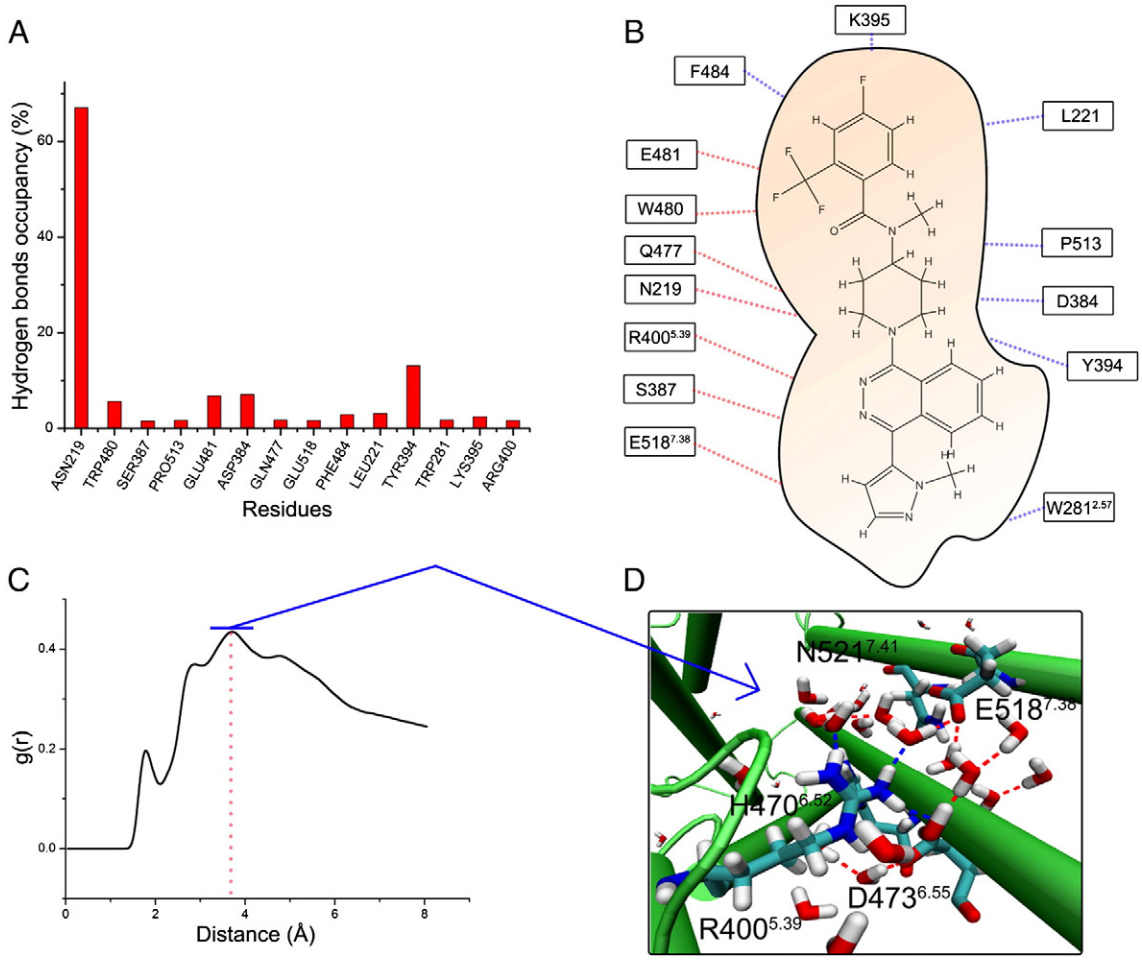

Fig. 6. The interaction mechanism between the antagonist LY2940680 and SMO receptor. (A) The hydrogen bond occupancy between the antagonist LY2940680 and the residues of SMO receptor. (B) The sites of SMO receptor formed hydrogen bonds with the antagonist LY2940680. The 3D representation of hydrogen bonds between SMO receptor and antagonist LY2940680 was shown in Fig. S3. (C) The radial distribution function $g(r)$ between the waters and R400$^{5.39}$, H470$^{6.52}$, D473$^{6.55}$, E518$^{7.38}$, N521$^{7.41}$. (D) The representation of hydrogen-bonding network between waters and R400$^{5.39}$, H470$^{6.52}$, D473$^{6.55}$, E518$^{7.38}$, N521$^{7.41}$.

bonds with antagonist LY2940680 (see Figs. 6A, B, and S1). To validate the conformational stability of K395, F484, E481, W480, Q477, N219, R400, S387, E518, W281, Y394, D384, P513, L221 and antagonist LY2940680, the RMSD was calculated on the basis of their backbone atoms. Fig. S4 showed that they could keep the dynamical equilibrium phase in the 50 ns simulation. The results of hydrogen bonds suggested that the ECD linker domain, ECL2, ECL3 and helixes II, V, VI, and VII formed the ligand-binding pocket of SMO receptor.

In the pocket of SMO receptor, the residues R400$^{5.39}$, H470$^{6.52}$, D473$^{6.55}$, E518$^{7.38}$ and N521$^{7.41}$ formed a hydrogen-bonding network with the water to stabilize the conformation and dynamics of the pocket [15]. To study the water distribution around these residues, $g(r)$ was employed to calculate the possibility along the reaction distance between the water molecules and residues R400$^{5.39}$, H470$^{6.52}$, D473$^{6.55}$, E518$^{7.38}$, N521$^{7.41}$ during 50 ns MD simulations (see Fig. 6C and D). The $g(r)$ had a peak value at the reaction distance of ~3.7 Å corresponding to the distance of hydrogen bonds. It indicated that the hydrogen-bonding network formed a dynamical interaction with the residues in the pocket of SMO receptor. With the increase of the reaction distance, the number of water in the pocket decreased, and the value of $g(r)$ also went down.

3.4. Metadynamics simulations

There were different dihedral rotation behaviors of the ligand in the solvation and protein environment. The study of these differences could get more details about the interaction mechanism between the receptor and ligand. To study the free energy of rotation of the antagonist LY2940680 in a solvation environment and SMO receptor, two systems were built for metadynamics: one (LY2940680–water) was the antagonist LY2940680 which immersed into the water box freely, the other (LY2940680–SMO) was the antagonist LY2940680 in complex with SMO receptor, explicit water, ions and lipids. As shown in Fig. 7A, the angles of θ_1 and θ_2 were rotated near the N219 of the ECD linker domain for the free energy surface computation of the antagonist LY2940680. There existed three obvious free energy surfaces in the LY2940680–water system. The predominant conformation of the antagonist LY2940680 in the LY2940680–water system matched with the θ_1 and θ_2 values of approximately [50° 150°] and [−180° −50°]. The [θ_1 θ_2] values corresponding to the pairwise dihedral angles of approximately [75° 125°], [50° 100°] and [50° 125°], [150° 180°] represented the minor conformation of the antagonist LY2940680. The other angles of [θ_1 θ_2] were unreachable because the methyl group could hinder the carbonyl and trifluoromethyl group of the antagonist LY2940680 during the angle rotation of metadynamics simulations (see Fig. 7A and C). Meanwhile, the LY2940680–SMO system only showed one energy surface in Fig. 7D. The predominant conformation of the antagonist LY2940680 corresponded to the [θ_1 θ_2] values of approximately [60° 150°] and [−170° −40°]. By comparing Fig. 7C with Fig. 7D, it was obvious that the most stable conformations corresponding to free energy values of 0 kcal/mol in Fig. 7D were distributed in a wider region

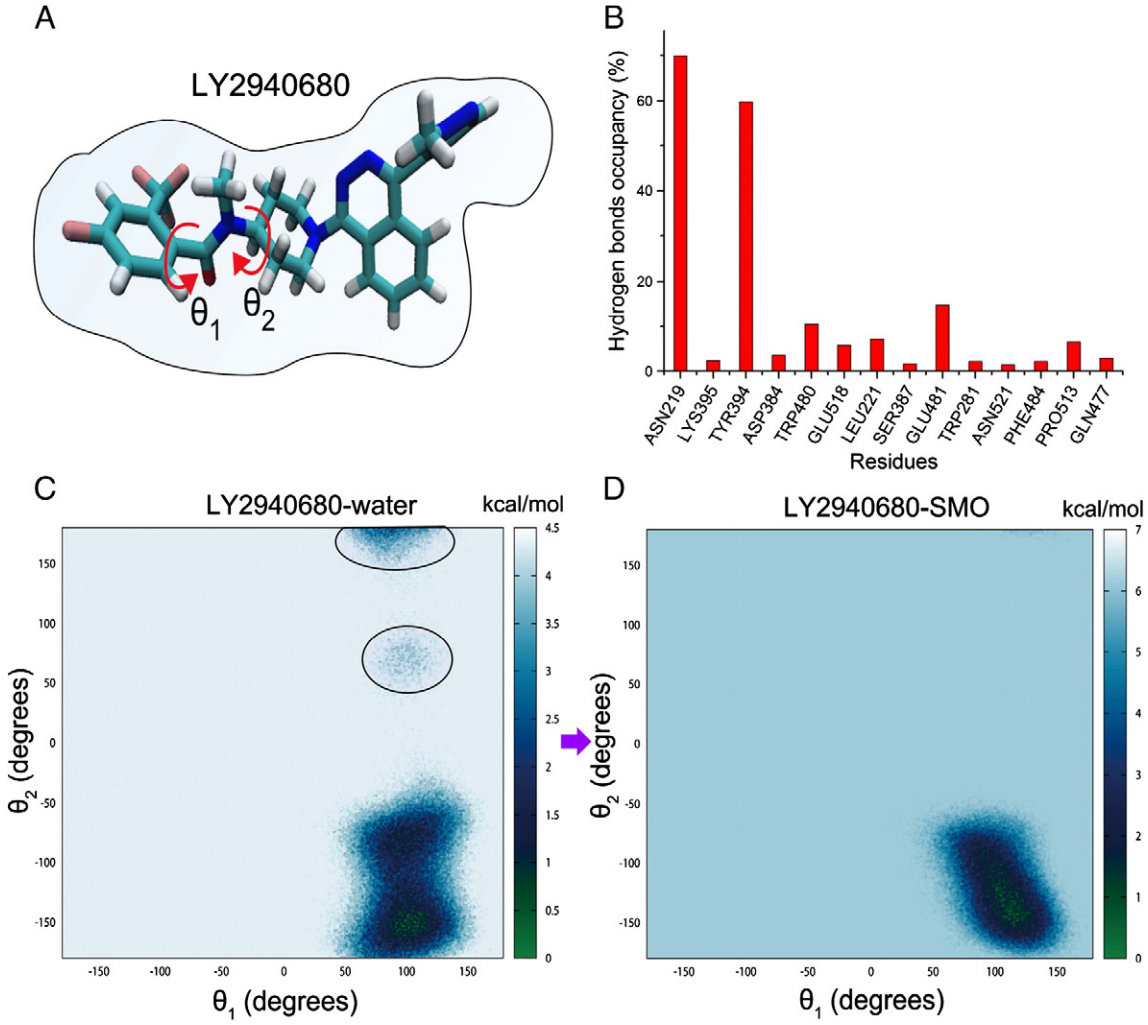

Fig. 7. The results from metadynamics simulations. (A) The sketch of rotated angles (θ_1 and θ_2) of metadynamics simulations. (B) The hydrogen bond occupancy between antagonist LY2940680 and the residues of SMO receptor during the metadynamics simulations. (C) Free energy surface of the antagonist LY2940680 in the bulk water using the θ_1 and θ_2 torsional angles as the reaction coordinate. (D) Free energy surface of the antagonist LY2940680 in complex with SMO receptor, ions and lipids.

than in Fig. 7C. It indicated that the residues of SMO receptor affected the conformation of the antagonist LY2940680 during the angle rotation of metadynamics simulation. As shown in Figs. 6A and 7B, the hydrogen bond occupancy between the antagonist LY2940680 and the residue R400$^{5.39}$ disappeared during the metadynamics simulations. Instead, the hydrogen bonds between the antagonist LY294068 and N521$^{7.41}$ which are located in the hydrogen-bonding network of water were kept. It indicated that the R400$^{5.39}$ was located in the binding site of the antagonist LY2940680. In addition, the hydrogen bond occupancy of Y394 in ECL2 increased during the metadynamics simulations. It suggested that the residue Y394 of ECL2 had a strong interaction with the antagonist LY2940680 along reaction coordinate during the metadynamics simulations. The results of metadynamics simulations provided useful information for drug design on the basis of the binding mode of the antagonist.

3.5. Free energy calculations

Since the free energy surface of rotation of the antagonist was studied in the pocket of SMO receptor, it was necessary to study the free energy of dissociation of antagonist LY2940680 in the pocket of SMO receptor. The ABF method could make the sampling in equal probability and improve the accuracy of free energy calculation by the reversibly calculated process. ABF simulation was used to explore the free energy when the antagonist LY2940680 escaped from the pocket of SMO receptor. As shown in Fig. 8A, the antagonist LY2940680 needed to conquer about 38 kcal/mol of energy barrier to get out the pocket of SMO receptor.

The energy barrier corresponding to the interaction between residues of SMO and the antagonist LY2940680 during the ABF simulations was shown in Fig. 8B and C. The hydrogen bond occupancy showed two important parts for the dissociation of the antagonist LY2940680, one was the residues in the ligand-binding pocket of SMO receptor including TYR394, ASN219, ILE215, ASP384, TYR207, GLU518$^{7.38}$, SER387, PHE484, GLU481 and LYS395, the other was in the region of the ECD linker domain, ECL1 and the α-helical extension of TM6 including ARG485, LEU197, VAL210, ASP209, VAL488, CYS213, GLN491, LEU489, LEU303, CYS193, GLN192, GLU211, GLY212, ARG199, THR200, TRP206 and ASP201. The antagonist LY2940680 should break the interaction with residues in the pocket of SMO receptor, and then left the pocket to the extracellular part of SMO receptor. Because the SMO receptor contained a long ECD linker domain, ECLs and the α-helical extension of TM6, the antagonist LY2940680 still interacted with SMO receptor directly though the antagonist got out of the pocket. The dynamically unbinding pathway of antagonist LY2940680 was illustrated in the Movie S1. The results of ABF simulations indicated that the ECD linker domain and α-helical extension of TM6 not only played an important role on the interaction between the antagonist LY2940680 and the residues in the pocket of SMO receptor, but also were relevant to the dissociation pathway of the antagonist LY2940680.

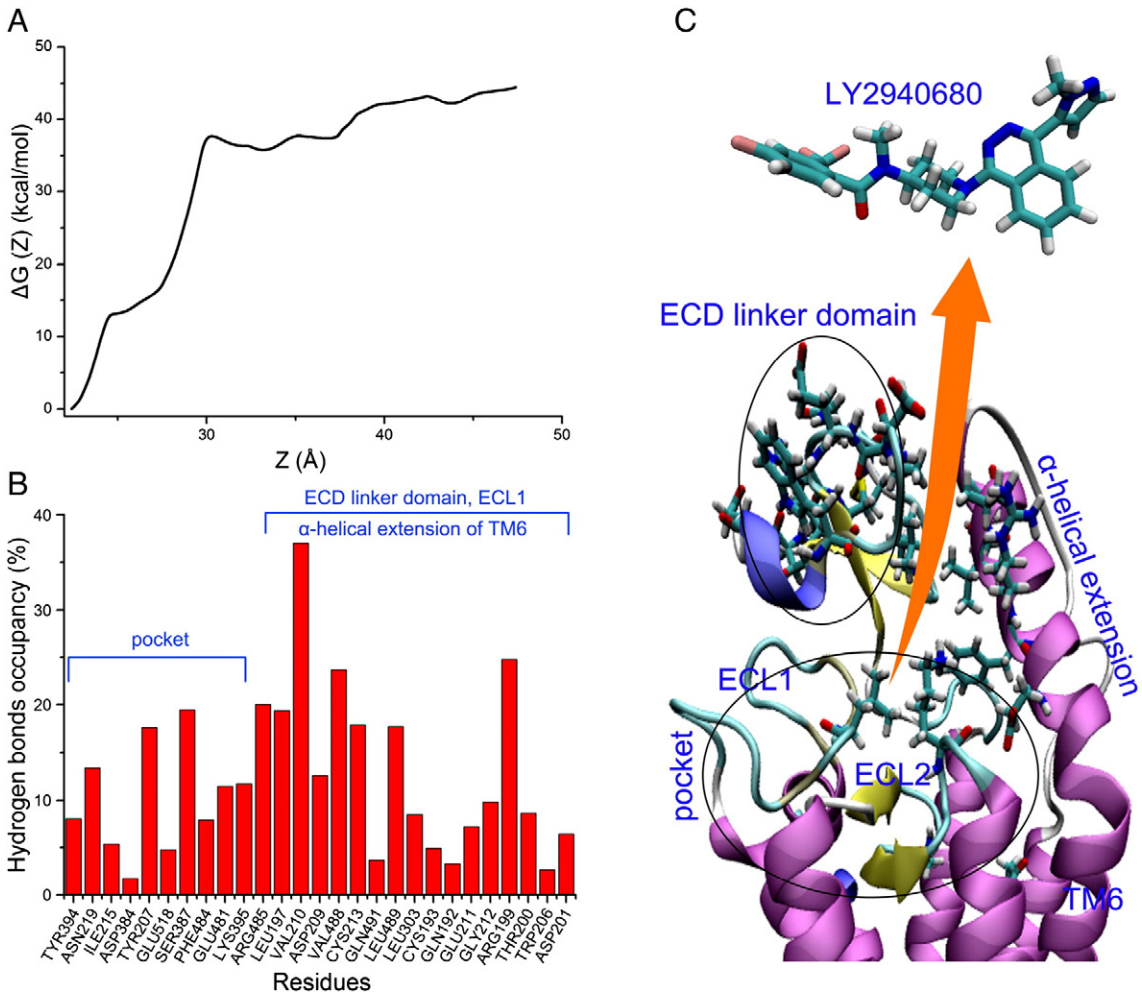

Fig. 8. The results of ABF simulations. (A) Free energy delineating the separation of the antagonist LY2940680 from the pocket of SMO receptor along the Z axis. (B) The hydrogen bond occupancy between the antagonist LY2940680 and pocket of SMO receptor along the reaction coordinate of ABF simulations. (C) The sketch of the residues of ECD linker domain, ECL1, α-helical extension of TM6 and the pocket of SMO receptor in the dissociation pathway of antagonist LY2940680.

4. Conclusions

In this work, we studied the dynamical structural features and interaction mechanism between the antagonist LY2940680 and SMO receptor by using MD simulations, dynamical network analysis, metadynamics simulations and ABF simulations. The simulation results showed that motif KTXXXW was included in the strongest edges and had different behaviors with the other residues of SMO receptor. The ECD linker domain, helixes II, V, and VII, and the α-helical extensions of TM6, ECL2 and ECL3 formed the antagonist-binding pocket. To study the binding mechanism of the antagonist in the pocket of SMO receptor, the metadynamics and ABF simulations were used to explore the free energy along the reaction coordinate of rotation and dissociation. The results of metadynamics indicated that conformation of the antagonist LY2940680 was restricted by the residues of SMO receptor. The ABF simulations proved that the antagonist LY2940680 needed to overcome about 38 kcal/mol of energy barrier to escape the pocket of SMO receptor along the dissociation pathway. Generally, our study not only provided the interaction mechanism between the antagonist and SMO receptor, but also gave useful information about the conformational features of the antagonist and SMO receptor for drug design.

Supplementary data to this article can be found online at http://dx.doi.org/10.1016/j.bbagen.2014.03.010.

Acknowledgements

This work was supported by the National Natural Science Foundation of China (Grant No. 21175063) and the program for Changjiang Scholars and Innovative Research Team in University (PCSIRT: IRT1137).

References

[1] J.P. Overington, B. Al-Lazikani, A.L. Hopkins, How many drug targets are there? Nat. Rev. Drug Discov. 5 (2006) 993–996.
[2] K. Hollenstein, J. Kean, A. Bortolato, R.K. Cheng, A.S. Dore, A. Jazayeri, R.M. Cooke, M. Weir, F.H. Marshall, Structure of class B GPCR corticotropin-releasing factor receptor 1, Nature 499 (2013) 438–443.
[3] U. Gether, Uncovering molecular mechanisms involved in activation of G protein-coupled receptors, Endocr. Rev. 21 (2000) 90–113.
[4] M.C. Lagerstrom, H.B. Schioth, Structural diversity of G protein-coupled receptors and significance for drug discovery, Nat. Rev. Drug Discov. 7 (2008) 339–357.
[5] A.J. Venkatakrishnan, X. Deupi, G. Lebon, C.G. Tate, G.F. Schertler, M.M. Babu, Molecular signatures of G-protein-coupled receptors, Nature 494 (2013) 185–194.
[6] T.K. Attwood, J.B. Findlay, Fingerprinting G-protein-coupled receptors, Protein Eng. 7 (1994) 195–203.
[7] L.F. Kolakowski Jr., GCRDb: a G-protein-coupled receptor database, Receptors Channels 2 (1994) 1–7.
[8] S.M. Foord, T.I. Bonner, R.R. Neubig, E.M. Rosser, J.P. Pin, A.P. Davenport, M. Spedding, A.J. Harmar, International Union of Pharmacology. XLVI. G protein-coupled receptor list, Pharmacol. Rev. 57 (2005) 279–288.
[9] D.M. Rosenbaum, S.G. Rasmussen, B.K. Kobilka, The structure and function of G-protein-coupled receptors, Nature 459 (2009) 356–363.
[10] F.Y. Siu, M. He, C. de Graaf, G.W. Han, D. Yang, Z. Zhang, C. Zhou, Q. Xu, D. Wacker, J.S. Joseph, W. Liu, J. Lau, V. Cherezov, V. Katritch, M.W. Wang, R.C. Stevens, Structure of the human glucagon class B G-protein-coupled receptor, Nature 499 (2013) 444–449.
[11] P.W. Ingham, A.P. McMahon, Hedgehog signaling in animal development: paradigms and principles, Genes Dev. 15 (2001) 3059–3087.
[12] D.J. Robbins, D.L. Fei, N.A. Riobo, The Hedgehog signal transduction network, Sci. Signal. 5 (2012) re6.
[13] K.L. Ayers, P.P. Therond, Evaluating Smoothened as a G-protein-coupled receptor for Hedgehog signalling, Trends Cell Biol. 20 (2010) 287–298.
[14] G. Schulte, International Union of Basic and Clinical Pharmacology. LXXX. The class Frizzled receptors, Pharmacol. Rev. 62 (2010) 632–667.
[15] C. Wang, H. Wu, V. Katritch, G.W. Han, X.P. Huang, W. Liu, F.Y. Siu, B.L. Roth, V. Cherezov, R.C. Stevens, Structure of the human smoothened receptor bound to an antitumour agent, Nature 497 (2013) 338–343.
[16] J. Taipale, J.K. Chen, M.K. Cooper, B. Wang, R.K. Mann, L. Milenkovic, M.P. Scott, P.A. Beachy, Effects of oncogenic mutations in Smoothened and Patched can be reversed by cyclopamine, Nature 406 (2000) 1005–1009.
[17] F. Fanelli, P.G. De Benedetti, Update 1 of: computational modeling approaches to structure–function analysis of G protein-coupled receptors, Chem. Rev. 111 (2011) R438–R535.
[18] F. Fanelli, P.G. De Benedetti, Computational modeling approaches to structure–function analysis of G protein-coupled receptors, Chem. Rev. 105 (2005) 3297–3351.
[19] S. Vanni, M. Neri, I. Tavernelli, U. Rothlisberger, Predicting novel binding modes of agonists to beta adrenergic receptors using all-atom molecular dynamics simulations, PLoS Comput. Biol. 7 (2011) e1001053.
[20] Q. Bai, Y. Zhang, Y. Ban, H. Liu, X. Yao, Computational study on the different ligands induced conformation change of beta2 adrenergic receptor–Gs protein complex, PLoS One 8 (2013) e68138.
[21] B. Isin, G. Estiu, O. Wiest, Z.N. Oltvai, Identifying ligand binding conformations of the beta2-adrenergic receptor by using its agonists as computational probes, PLoS One 7 (2012) e50186.
[22] R.O. Dror, A.C. Pan, D.H. Arlow, D.W. Borhani, P. Maragakis, Y. Shan, H. Xu, D.E. Shaw, Pathway and mechanism of drug binding to G-protein-coupled receptors, Proc. Natl. Acad. Sci. U. S. A. 108 (2011) 13118–13123.
[23] A. Gonzalez, T. Perez-Acle, L. Pardo, X. Deupi, Molecular basis of ligand dissociation in beta-adrenergic receptors, PLoS One 6 (2011) e23815.
[24] D. Provasi, M.C. Artacho, A. Negri, J.C. Mobarec, M. Filizola, Ligand-induced modulation of the free-energy landscape of G protein-coupled receptors explored by adaptive biasing techniques, PLoS Comput. Biol. 7 (2011) e1002193.
[25] R. Tripathi, N.N. Nair, Mechanism of acyl-enzyme complex formation from the Henry–Michaelis complex of class C beta-lactamases with beta-lactam antibiotics, J. Am. Chem. Soc. 135 (2013) 14679–14690.
[26] W. Zheng, A.V. Vargiu, M.A. Rohrdanz, P. Carloni, C. Clementi, Molecular recognition of DNA by ligands: roughness and complexity of the free energy profile, J. Chem. Phys. 139 (2013) 145102.
[27] A. Barducci, M. Bonomi, M.K. Prakash, M. Parrinello, Free-energy landscape of protein oligomerization from atomistic simulations, Proc. Natl. Acad. Sci. U. S. A. 110 (2013) E4708–E4713.
[28] P. Tiwary, M. Parrinello, From metadynamics to dynamics, Phys. Rev. Lett. 111 (2013) 230602.
[29] J. Li, A.L. Jonsson, T. Beuming, J.C. Shelley, G.A. Voth, Ligand-dependent activation and deactivation of the human adenosine A2A receptor, J. Am. Chem. Soc. 135 (2013) 8749–8759.
[30] R.O. Dror, D.H. Arlow, P. Maragakis, T.J. Mildorf, A.C. Pan, H. Xu, D.W. Borhani, D.E. Shaw, Activation mechanism of the beta2-adrenergic receptor, Proc. Natl. Acad. Sci. U. S. A. 108 (2011) 18684–18689.
[31] D.M. Rosenbaum, C. Zhang, J.A. Lyons, R. Holl, D. Aragao, D.H. Arlow, S.G. Rasmussen, H.J. Choi, B.T. Devree, R.K. Sunahara, P.S. Chae, S.H. Gellman, R.O. Dror, D.E. Shaw, W. I. Weis, M. Caffrey, P. Gmeiner, B.K. Kobilka, Structure and function of an irreversible agonist-beta(2) adrenoceptor complex, Nature 469 (2011) 236–240.
[32] Z. Feng, T. Hou, Y. Li, Studies on the interactions between beta2 adrenergic receptor and Gs protein by molecular dynamics simulations, J. Chem. Inf. Model. 52 (2012) 1005–1014.
[33] P. Kolb, D.M. Rosenbaum, J.J. Irwin, J.J. Fung, B.K. Kobilka, B.K. Shoichet, Structure-based discovery of beta2-adrenergic receptor ligands, Proc. Natl. Acad. Sci. U. S. A. 106 (2009) 6843–6848.
[34] W. Humphrey, A. Dalke, K. Schulten, VMD: visual molecular dynamics, J. Mol. Graph. 14 (1996) 33–38 (27–38).
[35] W.L. Jorgensen, J. Chandrasekhar, J.D. Madura, R.W. Impey, M.L. Klein, Comparison of simple potential functions for simulating liquid water, J. Chem. Phys. 79 (1983) 926–935.
[36] V. Zoete, M.A. Cuendet, A. Grosdidier, O. Michielin, SwissParam: a fast force field generation tool for small organic molecules, J. Comput. Chem. 32 (2011) 2359–2368.
[37] T. Darden, D. York, L. Pedersen, Particle mesh Ewald: An N [center-dot] log(N) method for Ewald sums in large systems, J. Chem. Phys. 98 (1993) 10089–10092.
[38] S.A. Adelman, J.D. Doll, Generalized Langevin equation approach for atom/solid-surface scattering: general formulation for classical scattering off harmonic solids, J. Chem. Phys. 64 (1976) 2375–2388.
[39] R.L. Davidchack, R. Handel, M.V. Tretyakov, Langevin thermostat for rigid body dynamics, J. Chem. Phys. 130 (2009) 234101.
[40] S.E. Feller, Y. Zhang, R.W. Pastor, B.R. Brooks, Constant pressure molecular dynamics simulation: the Langevin piston method, J. Chem. Phys. 103 (1995) 4613–4621.
[41] J.C. Phillips, R. Braun, W. Wang, J. Gumbart, E. Tajkhorshid, E. Villa, C. Chipot, R.D. Skeel, L. Kale, K. Schulten, Scalable molecular dynamics with NAMD, J. Comput. Chem. 26 (2005) 1781–1802.
[42] J. Eargle, Z. Luthey-Schulten, NetworkView: 3D display and analysis of protein.RNA interaction networks, Bioinformatics 28 (2012) 3000–3001.
[43] A. Sethi, J. Eargle, A.A. Black, Z. Luthey-Schulten, Dynamical networks in tRNA:protein complexes, Proc. Natl. Acad. Sci. U. S. A. 106 (2009) 6620–6625.
[44] N.M. Glykos, Software news and updates. Carma: a molecular dynamics analysis program, J. Comput. Chem. 27 (2006) 1765–1768.
[45] B. Roux, The calculation of the potential of mean force using computer simulations, Comput. Phys. Commun. 91 (1995) 275–282.
[46] J.G. Kirkwood, Statistical mechanics of fluid mixtures, J. Chem. Phys. 3 (1935) 300–313.
[47] S.K. Sadiq, F. Noe, G. De Fabritiis, Kinetic characterization of the critical step in HIV-1 protease maturation, Proc. Natl. Acad. Sci. U. S. A. 109 (2012) 20449–20454.
[48] E. Espinosa, E. Molins, C. Lecomte, Hydrogen bond strengths revealed by topological analyses of experimentally observed electron densities, Chem. Phys. Lett. 285 (1998) 170–173.
[49] Q. Bai, Y. Shen, X. Yao, F. Wang, Y. Du, Q. Wang, N. Jin, J. Hai, T. Hu, J. Yang, Modeling a new water channel that allows SET9 to dimethylate p53, PLoS One 6 (2011) e19856.
[50] B.G. Levine, J.E. Stone, A. Kohlmeyer, Fast analysis of molecular dynamics trajectories with graphics processing units—radial distribution function histogramming, J. Comput. Phys. 230 (2011) 3556–3569.

[51] A. Laio, M. Parrinello, Escaping free-energy minima, Proc. Natl. Acad. Sci. U. S. A. 99 (2002) 12562–12566.
[52] H.S. Hansen, P.H. Hunenberger, Using the local elevation method to construct optimized umbrella sampling potentials: calculation of the relative free energies and interconversion barriers of glucopyranose ring conformers in water, J. Comput. Chem. 31 (2010) 1–23.
[53] E. Darve, D. Rodriguez-Gomez, A. Pohorille, Adaptive biasing force method for scalar and vector free energy calculations, J. Chem. Phys. 128 (2008) 144120.
[54] E. Darve, A. Pohorille, Calculating free energies using average force, J. Chem. Phys. 115 (2001) 9169–9183.
[55] J.r. Hénin, G. Fiorin, C. Chipot, M.L. Klein, Exploring multidimensional free energy landscapes using time-dependent biases on collective variables, J. Chem. Theory Comput. 6 (2009) 35–47.
[56] A. Laio, F.L. Gervasio, Metadynamics: a method to simulate rare events and reconstruct the free energy in biophysics, chemistry and material science, Rep. Prog. Phys. 71 (2008) 126601.
[57] F. Dehez, E. Pebay-Peyroula, C. Chipot, Binding of ADP in the mitochondrial ADP/ATP carrier is driven by an electrostatic funnel, J. Am. Chem. Soc. 130 (2008) 12725–12733.
[58] D. Wacker, G. Fenalti, M.A. Brown, V. Katritch, R. Abagyan, V. Cherezov, R.C. Stevens, Conserved binding mode of human beta2 adrenergic receptor inverse agonists and antagonist revealed by X-ray crystallography, J. Am. Chem. Soc. 132 (2010) 11443–11445.
[59] C.E. Carroll, S. Marada, D.P. Stewart, J.X. Ouyang, S.K. Ogden, The extracellular loops of Smoothened play a regulatory role in control of Hedgehog pathway activation, Development 139 (2012) 612–621.
[60] B. Knapp, N. Lederer, U. Omasits, W. Schreiner, vmdICE: a plug-in for rapid evaluation of molecular dynamics simulations using VMD, J. Comput. Chem. 31 (2010) 2868–2873.
[61] S.A.M. Stein, A.E. Loccisano, S.M. Firestine, J.D. Evanseck, Chapter 13 Principal components analysis: a review of its application on molecular dynamics data, in: C.S. David (Ed.), Annual Reports in Computational Chemistry, vol. 2, Elsevier, 2006, pp. 233–261